Provided for non-commercial research and education use.
Not for reproduction, distribution or commercial use.

This article was published in an Elsevier journal. The attached copy is furnished to the author for non-commercial research and education use, including for instruction at the author's institution, sharing with colleagues and providing to institution administration.

Other uses, including reproduction and distribution, or selling or licensing copies, or posting to personal, institutional or third party websites are prohibited.

In most cases authors are permitted to post their version of the article (e.g. in Word or Tex form) to their personal website or institutional repository. Authors requiring further information regarding Elsevier's archiving and manuscript policies are encouraged to visit:

http://www.elsevier.com/copyright

Author's personal copy

ELSEVIER

Microelectronics Journal 39 (2008) 601–606

Microelectronics Journal

www.elsevier.com/locate/mejo

Semiconductor terahertz detectors and absorption enhancement using plasmons

A.G.U. Perera[a,*], G. Ariyawansa[a], P.V.V. Jayaweera[a], S.G. Matsik[a], M. Buchanan[b], H.C. Liu[b]

[a]*Department of Physics and Astronomy, Georgia State University,Atlanta, GA 30303, USA*
[b]*Institute for Microstructural Sciences, National Research Council, Ottawa, Canada K1A OR6*

Available online 4 September 2007

Abstract

As novel applications using terahertz radiation are developed, there is an increased demand for sensitive terahertz detectors. This has led to new approaches for enhancing the response of terahertz detectors. Results were recently reported on the terahertz response of a p-type AlGaAs/GaAs, n-type GaAs/AlGaAs, n-type GaN/AlGaN, and p-type GaSb/GaSb Interfacial Workfunction Internal Photoemission detectors. The use of surface plasmon coupling due to metal grids is one approach discussed here to enhance the performance of these terahertz detectors. Due to the greatly enhanced near fields of the plasmons, the absorption would be increased leading to improved detectors. Results are presented on the enhancement of absorption by plasmon effects in a thin film coupled with a metal grid.
© 2007 Elsevier Ltd. All rights reserved.

Keywords: GaAs/AlGaAs devices; GaN/AlGaN devices; GaSb devices; Terahertz detectors; Surface plasmons

1. Introduction

The use of terahertz radiation as a tool for exploring materials has been widely demonstrated. Applications can be found in various fields such as medicine, industry, security, astronomy, and atmospheric studies. Some examples include cancer/tumor detection, non-destructive testing [1], toxic/chemical detection, and gas sensing. The key advantage of terahertz radiation in these areas is the ability to penetrate and distinguish between non-metallic materials. The terahertz range is especially useful in gas sensing, where a terahertz detector can be coupled with a laser emitting at the frequency of the absorption line of the gas (fingerprint of the gas), because the fingerprints of large number of gases fall in the range of 0.5–3 THz. In order to satisfy the requirements of developing terahertz technology, however, fast highly sensitive terahertz detectors operating at high temperatures have not been developed yet. Present detectors which are in operation are based on gated antennae [2], thermal detectors such as bolometers and pyroelectric detectors Ge BIB detectors [3], and photoconductors triggered by femtosecond laser pulses [4]. Recently, a 6 THz tunneling quantum dot detector [5] operating at 150 K was demonstrated. Also HEterojunction/Homojunction Interfacial Workfunction Internal Photoemission (HEIWIP/HIWIP) detectors have shown promising results indicating the feasibility of next generation terahertz detectors. In this article, a comparative discussion on several previously reported HEIWIP terahertz detectors based on p-type AlGaAs/GaAs [6], n-type GaAs/AlGaAs [7], and n-type GaN/AlGaN [8] material systems, and a p-type GaSb/GaSb [9] based HIWIP terahertz detector is presented. The major problem of these detectors is the low quantum efficiency, which is primarily due to low radiation absorption in the terahertz region. One approach to overcome this problem is the use of surface plasmon to enhance terahertz radiation absorption in the active layer of the structure. Preliminary experimental results and theoretical modeling of surface plasmon effects are discussed.

*Corresponding author. Tel.: +1 404 651 2847; fax: +1 404 651 1427.
E-mail address: uperera@gsu.edu (A.G.U. Perera).

0026-2692/$ - see front matter © 2007 Elsevier Ltd. All rights reserved.
doi:10.1016/j.mejo.2007.07.086

Author's personal copy

2. HIWIP/HEIWIP structures: background

HIWIP/HEIWIP infrared (IR) detectors based on the p-type GaAs/AlGaAs system have been successfully demonstrated [10–13] with tailorable wavelength threshold (λ_0) of 20−92 μm. A typical HIWIP or HEIWIP detector consists of a single (or series of) doped emitter(s) followed by an undoped barrier(s), which are in turn sandwiched in two highly doped contact layers. The difference between HIWIP and HEIWIP is that both the emitter and barrier in a HIWIP structure are made of the same material but with higher doping in the emitter, while in a HEIWIP structure the emitter and the barrier are made of materials with different bandgaps. A schematic diagram of the layer architecture of a p-type HEIWIP structure is shown in Fig. 1(a). The detection mechanism is a three-stage process: free carrier absorption of the incoming photons in the emitter, internal photoemission, and collection of emitted carriers by an applied electric field across the contacts. For the free carrier absorption, both the initial and final carrier states are part of the same continuum, resulting in a response that is inherently broadband. The limit on the response wavelength is introduced in the photoemission stage. The emitter–barrier junction introduces a workfunction (Δ), which corresponds to the energy difference between top of the barrier and the Fermi level in the emitter. Carriers in the emitter with sufficient energy to pass over the barrier (with energy $>\Delta$) will escape the emitter, and can be collected at the contact by an applied electric field, as shown in Fig. 1(b). The λ_0 of the detector (in μm) is determined as $\lambda_0 = 1240/\Delta$ where Δ is in meV. Here, $\Delta = \Delta_x + \Delta_d$ for HEIWIP, and $\Delta = \Delta_d$ for HIWIP, where Δ_x is the workfunction due to band offset of the emitter and the barrier materials, and Δ_d is the workfunction due to bandgap narrowing from the doping in the emitter. By reducing the alloy fraction or the doping concentration of the layers, Δ can be reduced, tailoring λ_0 to the desired value. A detailed explanation on designing and optimization of HIWIP/HEIWIP detectors can be found in Refs. [10,12].

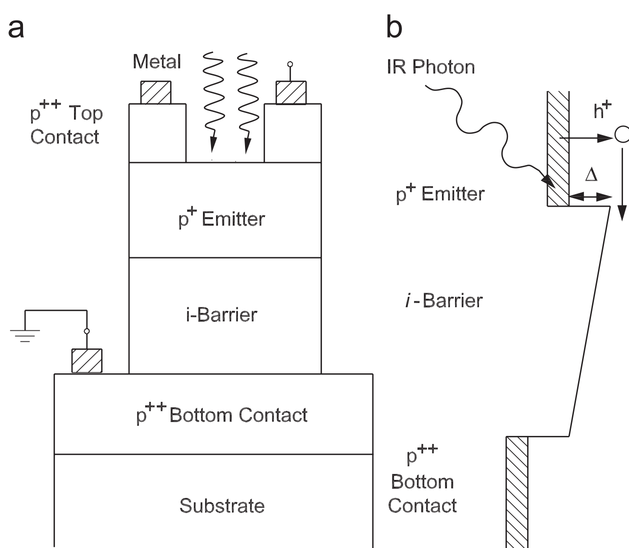

Fig. 1. (a) Schematic diagram of a p-type HEIWIP structure. The emitter is p-type doped and the contact layers are highly doped. The barrier is not intentionally doped. (b) Band diagram showing the valence band profiles of the structure under an electric field. The work function (Δ) in also indicated.

3. HIWIP/HEIWIP detectors for terahertz radiation detection

In general, HEIWIP detectors can be developed with any semiconductor material system such as, GaAs/AlGaAs, GaN/AlGaN, GaSb/AlGaSb, etc. However, choosing the material system and type of doping (n or p) depends on the present level of the growth quality of the material system, feasibility to obtain the response wavelength threshold, expected performance, as well as the possibilities of enhancing the performance. A comparison of the performance of several recently reported HIWIP/HEIWIP detectors, p-type AlGaAs/GaAs, n-type GaAs/AlGaAs, and n-type GaN/AlGaN, and p-type GaSb/GaSb, is presented in this section. The layer parameters of these structures are given in Table 1.

3.1. p-AlGaAs/GaAs HEIWIP terahertz detector

While Δ decreases with decreasing alloy fraction of the layer (x), tailoring the frequency threshold (f_0) to any desired value has been limited by the practical value of $x = 0.005$ for GaAs/AlGaAs (GaAs emitter/AlGaAs barrier) HEIWIPs [13] limiting the f_0 to 3.3 THz. On the other hand, for HIWIPs, f_0 is limited to 3 THz by the emitter doping concentration [14]. These limits of f_0 can be overcome by incorporating a doped $Al_xGa_{1-x}As$ emitter and an undoped GaAs barrier in the HEIWIP structure (i.e. AlGaAs/GaAs HEIWIP) allowing f_0 down to 1 THz. This approach was recently reported [6] with a AlGaAs/GaAs HEIWIP detector showing a f_0 of 2.3 THz. As explained in the Section 2, the $\Delta = \Delta_x + \Delta_d$ for HEIWIPs, and $\Delta_x > 0$ for GaAs/AlGaAs HEIWIPs. For AlGaAs/GaAs HEIWIPs, $\Delta_x < 0$ and therefore Δ can be reduced further, reducing the f_0 below 3.3 THz limit. However, due to residual doping in the barrier, Δ is modified such that $\Delta = \Delta_x + \Delta_d + \Delta_b$, where Δ_b (~13 meV at 0 V bias for the structure V0207 with layer parameters in Table 1), which decreases with the bias, is the contribution from band bending. The dependence of the responsivity of the detector (V0207) on the applied bias field is shown in Fig. 2. The calculated response is also shown in the figure. The vertical arrows indicate f_0 under each bias field. The shift of f_0 with the bias is due to the dependence of Δ_b with bias. As the bias increases, Δ_b decreases reducing effective Δ and reducing f_0 to 2.3 THz at 2 kV/cm field. This proves the idea that the limitation of f_0 due to growth issues can be overcome with AlGaAs/GaAs HEIWIPs.

Author's personal copy

Table 1
Layer parameters of different terahertz structures

Sample number	Emitter	x %	Barrier	N	w_{TC} µm	n_{TC} 10^{18} cm^{-3}	w_{EM} µm	n_{EM} 10^{18} cm^{-3}	w_B µm	w_{BC} µm	n_{BC} 10^{18}cm^{-3}
V0207	p-AlGaAs	0.5	GaAs	10	0.5	10	0.5	3	2	7	10
HE0501	n-GaAs	4	AlGaAs	1	0.1	1	–	–	1	0.7	1
B1158	n-GaN	2.6	AlGaN	1	0.2	5	–	–	0.6	0.7	5
GSU-A3	p-GaSb	0	GaSb	1	0.1	5	0.05	2	2	0.05	2

Here, N is the number of periods, w is the width of the layer, n is the doping concentration, and x is the alloy fraction in the emitter or barrier. TC, EM,B, and BC stand for top-contact, emitter, barrier, and bottom-contact. For HE501 and B1158 samples, the top-contact acts as the emitter.

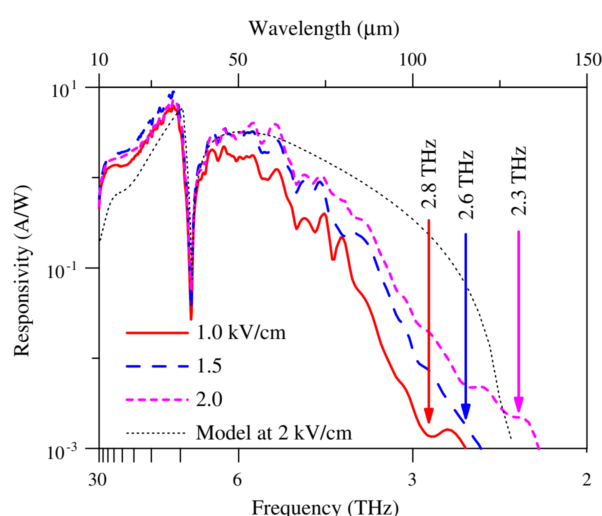

Fig. 2. The variation of responsivity with applied field for p-AlGaAs/GaAs HEIWIP (sample V0207) at 4.8 K. Increasing the bias field decreases the effective work function lowering f_0 to ~2 THz. Calculated responsivity at 2 kV/cm bias is shown by the dotted line. The dip in the responsivity curve at ~8.3 THz is due to GaAs-like optical phonons in the structure.

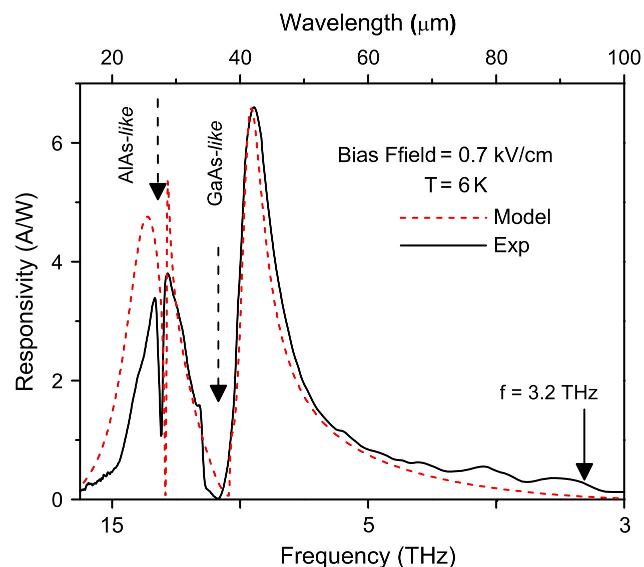

Fig. 3. Experimental and calculated responsivities of the n-GaAs/AlGaAs HEIWIP detector (sample HE0501) at 0.7 kV/cm and 6 K. Under this bias condition, the bottom contact acts as the emitter. The reduction of the experimental responsivity in the high-frequency region (>8 THz) could be due to phonon emission by high-energy photocarriers and energy-dependent scattering lengths.

3.2. n-GaAs/AlGaAs HEIWIP terahertz detector

Recently, an n-GaAs/AlGaAs HEIWIP detector was reported [7]. In comparison to p-GaAs/AlGaAs HEIWIPs, the Fermi level (E_F) in n-type HEIWIP structures shows a higher variation with the doping concentration in the emitter. Since electron effective mass is much lower than the hole effective mass, (E_F) changes more rapidly with carrier concentration in the n-type material. As explained in Section 2, $\Delta = \Delta_x + \Delta_d$ for HEIWIP, where Δ_d which corresponds to doping can be expanded such that $\Delta_d = \Delta_{narr} - E_F$ (Δ_{narr} is the band gap narrowing due to doping). Hence, using n-type GaAs/AlGaAs and controlling the doping concentration (i.e. controlling E_F) can lead to development of terahertz detectors with $f_0 = 1$ THz without the restriction by the practical limit of Al fraction. Experimental and calculated responsivities of an n-GaAs/AlGaAs HEIWIP detector (sample HE0501) are shown in Fig. 3. The layer parameters are given in Table 1. The frequency threshold observed is 3.2 THz and this does not change with the applied bias, implying that there is little space charge buildup on the interface, as expected. Two dips at around 11 and 8.3 THz are due to AlAs-like and GaAs-like optical phonons in the AlGaAs layer. The reduction of the experimental responsivity in the high-frequency region (>8 THz) could be due to phonon emission by high-energy photocarriers and energy-dependent scattering lengths. In comparison to p-type GaAs/AlGaAs, which showed a 3.2 THz threshold with x of 0.005, the practical limit, demonstrating the same threshold with x of 0.04, n-type HEIWIPs shows the feasibility of developing terahertz detectors with threshold at around 1 THz.

3.3. n-GaN/AlGaN HEIWIP terahertz detectors

Due to the fast development of the GaN/AlGaN material system, a preliminary GaN/AlGaN HEIWIP detector was developed and promising results were recently reported [8]. The detector structure was grown by OMCVD

Author's personal copy

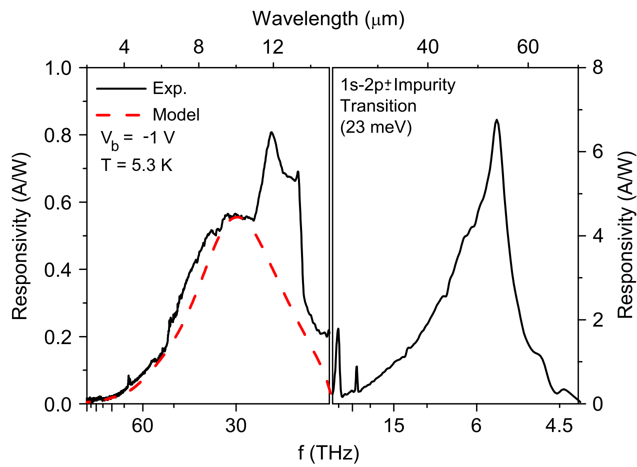

Fig. 4. A comparison between the experimental and calculated free carrier response of n-GaN/AlGaN HEIWIP detector (sample B1158) at −1 V and 5.3 K. The sharp features in the 11−13 μm range can be due to impurity transitions of Carbon impurity atoms or Nitrogen vacancies. The sharp peak at 5.5 THz (54 μm) was identified as 1s−2p± transitions of Si impurity atoms in the structure. The origin of the terahertz response has not been identified yet.

on a Sapphire substrate and the layer parameters are given in Table 1. A comparison between the experimental and calculated responses is shown in Fig. 4. The free carrier response in the experimental curves is in good agreement with the model below 11 μm. An additional feature in the range of 11−13 μm was observed in the experimental curve. This feature has been identified as due to a combination of Carbon impurities, which are present in OMCVD grown structures, and Nitrogen vacancies. The sharp peak at 5.5 THz (54 μm), shown in Fig. 4, is due to the 1s−2p± transition of silicon (Si) dopant atoms, which has been observed previously [15] with the same energy of ∼23 meV. Based on this preliminary results for the unoptimized detector structure, it is expected that terahertz detectors can be developed with GaN/AlGaN HEIWIP structures.

3.4. p-GaSb/GaSb HIWIP terahertz detector

In HIWIPs, Δ can be varied by $\Delta_d = \Delta_{\text{narr}} - E_{\text{F}}$, where Δ_{narr} and E_{F} vary with the doping concentration in the emitter. As a primary step of developing GaSb/InGaSb HEIWIP terahertz detectors, a p-GaSb/GaSb HIWIP detector with a f_0 of 3.1 THz was recently demonstrated [9]. The single period structure (layer parameters are given in Table 1) showed a free carrier response with a threshold at 3.1 THz and a flat response in the range 3–1.5 THz, as shown in Fig. 5. The sharp dip at ∼7 THz (43 μm) is due to reststrahlen absorption in GaSb. Based on the Arrhenius calculation, the activation energy was obtained to be 128 meV, which is in good agreement with the observed threshold (3.1 THz). The flat response in the range 3–1.5 THz is relatively weak compared to the free carrier response, but is an order of magnitude higher than the system noise level as shown in the figure. However, the origin of this peak has not been identified yet.

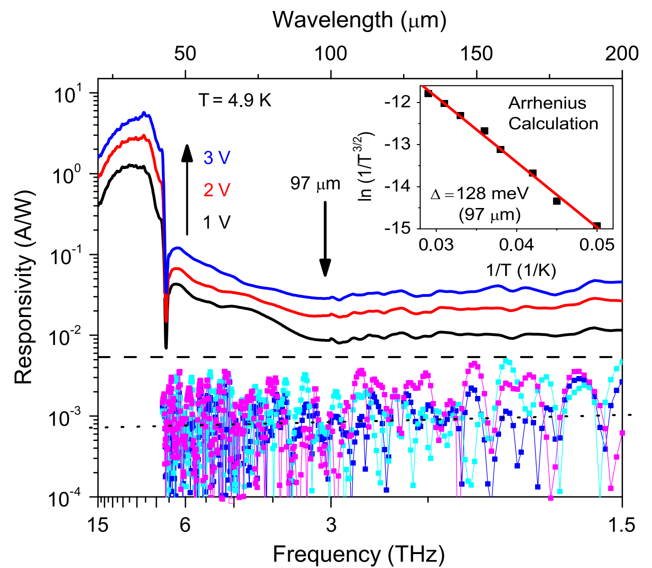

Fig. 5. The response of an p-GaSb/GaSb HIWIP detector (sample GSU-A3) in the 15–1.5 THz range at 1, 2, and 3 V bias voltages at 4.9 K. The arrow indicates free carrier wavelength threshold at the 97 μm. The noise curves at the bottom were obtained under dark conditions, and the dashed line shows the maximum noise level of the spectral response measurement setup. The Arrhenius curve, which translates to a activation energy of 128 meV (97 μm) is also shown in the inset.

Table 2
Detector parameters of different terahertz structures

Sample number	Material system	f_0 THz	R_P A/W	η %	D^* Jones
V0207	p-AlGaAs/GaAs	2.3	7.3	29	5.3×10^{11}
HE0501	n-GaAs/AlGaAs	3.2	6.5	19	5.5×10^{8}
B1158	n-GaN/AlGaN	21*	0.8	8	2.5×10^{10}
GSU-A3	p-GaSb/GaSb	3	9.7	33	5.7×10^{11}

Here, f_0 is the threshold frequency, R_P is the peak responsivity, η is the quantum efficiency, and D^* is the detectivity. * The f_0 corresponding to the free carrier response, while this detector shows an impurity response at 5.4 THz.

The promising results on a single period detector implies the possibility of developing GaSb/InGaSb HEIWIP terahertz detectors, which would provide more flexibility to control the threshold over the In fraction. Based on the lower band gap offset between GaSb and InSb, it is clear that f_0 of 1 THz could be achieved, while keeping the In fraction in the practical range. Therefore, GaSb based HEIWIPs would be a good substitution for GaAs or GaN based HEIWIPs, where high accuracy of x is needed to control the threshold.

The detector parameters for all the HIWIP and HEIWIP structures discussed are given in Table 2. In order to improve the performance of these HEIWIP detectors, using multi period structures and resonant cavity enhancement [16] have already been reported. In this article, another approach where the absorption of radiation in the active layer is enhanced by surface plasmon effects, is discussed.

Author's personal copy

4. Absorption enhancement by surface plasmon

The plasmon effect works by enhancing the optical electric field, hence enhancing the absorption. Electromagnetic waves at metal-dielectric or metal-semiconductor interfaces, such as surface plasmon polaritons, and surface plasmons, have remarkable properties of generating highly enhanced local fields [17,18]. These local fields in nanostructured systems can exceed excitation fields by orders of magnitude and undergo giant fluctuations in space [19] and in time [20]. These giant local fields are responsible for a multitude of enhanced optical phenomena and their applications [18,21]. Here, the idea for enhancing the performance of HEIWIP structures is to increase the absorption in the active region (emitter) of the structure by surface plasmon effects from a metal grid (grating) coupled to the emitter.

Plasmon interactions and their effects on reflection from ruled metal gratings have been observed since the original experimental work conducted by Woods [22]. The condition for plasmon formation by incident radiation of wavelength λ in this type of system is,

$$\frac{1}{\lambda}\sin\theta + \frac{n}{a} = \frac{1}{\lambda}\sqrt{\frac{\varepsilon_1\varepsilon_2}{\varepsilon_1+\varepsilon_2}}, \quad (1)$$

where θ is the incidence angle of the light, a is the grating period, ε_1 and ε_2 are the dielectric constants for the metal and the layer just above it, respectively, and n is an integer. The plasmon effects from this type of ruled metal grating formed on top of the HEIWIP structure will not enhance the absorption in the emitter, since the metal covers the entire surface and the formation of the plasmon takes place on the metal surface. That is, the plasmon fields are localized on the top of the grating, and hence they cannot serve to excite the carriers in the detector. Therefore, different types of surfaces with narrow slits in the grating have been considered in order to obtain better plasmon effects. For coupling the plasmons to a detector, openings are desired so that the plasmons will propagate around the metal to the bottom where they can couple to the detector. There has been some work on using grids with equal widths of metal and openings to couple GHz radiation to quantum well structures [23].

The two key factors to be considered are: (i) matching the size and shape of the metal pattern so the desired incident wavelength will generate plasmons, and (ii) the coupling of the plasmons to the detector. The generation of plasmons depends very significantly on the metallic pattern. To understand plasmon effects, a linear grid pattern with equal widths of metal strips and openings on a SiO_2 layer as shown in Fig. 6 was considered. In this pattern, only the radiation with the electric field perpendicular to the grid lines (p-polarization) is expected to couple to the plasmons. Three samples with grid periods of 2.8, 3.6, and 4.5 μm and a sample without a grid were fabricated, and transmission (T) and reflection measurements (R) were performed using a Fourier transform infrared spectrometer. The normalized absorption, $A = (1-T-R)/(1-R)$, which represents the fraction of the non-reflected radiation that is absorbed in the layer was obtained from these measurements. This definition of absorption is more closely related to the absorption coefficient, and the plasmon features for 3.6, and 4.5 μm period grids can be clearly observed in the absorption spectra. The normalized absorption results for the oxide layer without the grid and for grids with periods 2.8, 3.6, and 4.5 μm using incident radiation at an angle of 9° for p-polarized light are shown in Fig. 7. The plasmon features are indicated by the arrows. These features were observed only for the p-polarized light, as expected.

The peaks near 9 and 12 μm, which do not vary with the grid period, can be excluded since these features are not due to plasmon effects and can also be observed in the sample without the grid pattern. These features are probably due to the oxide layer. The peak shifting from 11 to 14 μm (indicated by the vertical arrows in Fig. 7) as the grid period is increased from 3.6 to 4.5 μm can be identified as plasmon features. However, this peak for the 3.6 μm period grid occurs near the minimum of the 9 and 12 μm features, appearing as a shoulder on the peak near 9 μm. Also the peak for the 4.5 μm period grid is near 14 μm and is not fully resolved from the stationary peak at 12 μm. The plasmon absorption peak for the sample

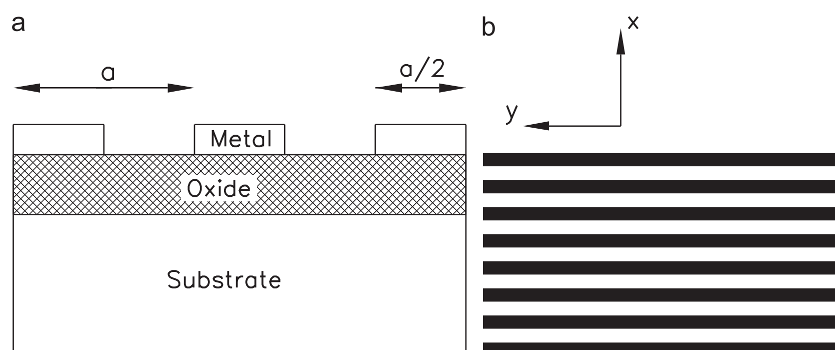

Fig. 6. (a) Side view showing the metal grid pattern on SiO_2 layer with the grid period a indicated. (b) A top view of the grid showing the equal metal and open areas. The arrows indicate the polarization directions for s and p polarized radiations relative to the grid.

Author's personal copy

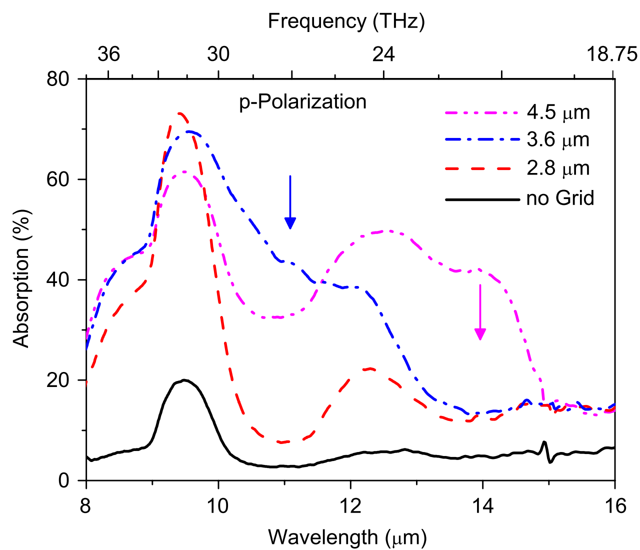

Fig. 7. A comparison between the absorption in the samples with different grid spacing and the sample without a grid pattern under p-polarized light at an incidence angle of 9°. The absorption peaks (indicated by the arrows) shift from 11 to 14 μm as the grid period is increased from 3.6 to 4.5 μm. Note the absorption peak for the 3.6 μm grid is superimposed on the oxide minimum, hence it appears as a filling of the minimum.

with 2.8 μm period grid is completely suppressed by the stationary absorption minima of the oxide layer. These wavelength locations agree well with the calculated values by Eq. (1) for a value of $\sqrt{\varepsilon_1\varepsilon_2/(\varepsilon_1+\varepsilon_2)} = 3.1$ with $n = 1$. Based on this result, it is apparent that by adjusting the grid parameters, the plasmon enhancement can be tuned to the desired wavelength region giving improved responsivity.

5. Conclusion

A comparative discussion of several previously reported HIWIP/HEIWIP detectors, p-type AlGaAs/GaAs, n-type GaAs/AlGaAs, and n-type GaN/AlGaN, and p-type GaSb/GaSb, was presented. Based on the results, it can be concluded that different material systems can be used to develop HEIWIP terahertz detectors. In order to improve the response, the use of surface plasmon effects was suggested. Experimental results were presented showing increased absorption due to plasmon effects in a metal grid. The wavelength for the plasmon effect can be tailored by adjusting the period of the metal grid. This effect could increase the sensitivity of HEIWIP detectors by a factor of five.

Acknowledgments

This work is supported in part by U.S. National Science Foundation (NSF) under Grant ECS-0553051 and Georgia Research Alliance under contract GRA. IC07.C. The authors would like to acknowledge Drs. N. Dietz, D. Huang, and D. Cardimona for fruitful discussions.

References

[1] P.H. Siegel, IEEE Trans. Microwave Theory Techniques 50 (2002) 910–928.
[2] J.W. Odendaal, J. Joubert, Electron. Lett. 35 (1999) 1894.
[3] E.E. Haller, Infrared Phys. 35 (1994) 127.
[4] M. Suzuki, M. Tonouchi, Appl. Phys. Lett. 86 (2005) 163504-1–163504-3.
[5] X.H. Su, J. Yang, P. Bhattacharya, G. Ariyawansa, A.G.U. Perera, Appl. Phys. Lett. 89 (2006) 031117.
[6] M.B.M. Rinzan, A.G.U. Perera, S.G. Matsik, H.C. Liu, Z.R. Wasilewski, M. Buchanan, Appl. Phys. Lett. 86 (2005) 071112.
[7] A. Weerasekara, M. Rinzan, S. Matsik, A.G.U. Perera, M. Buchanan, H.C. Liu, G. von Winckel, A. Stintz, S. Krishna, Optics Letters 32, 2007, 1335–1337.
[8] G. Ariyawansa, M.B.M. Rinzan, M. Strassburg, N. Dietz, A.G.U. Perera, S.G. Matsik, A. Asghar, I.T. Ferguson, H. Luo, H.C. Liu, Appl. Phys. Lett. 89 (2006) 141122-1–141122-3.
[9] P.V.V. Jayaweera, S.G. Matsik, A.G.U. Perera, Y. Paltiel, A. Sher, A. Raizman, H. Luo, H.C. Liu, Appl. Phys. Lett. 90 (2007) 111109-1–111109-3.
[10] W.Z. Shen, A.G.U. Perera, H.C. Liu, M. Buchanan, W.J. Schaff, Appl. Phys. Lett. 71 (1997) 2677.
[11] D.G. Esaev, M.B.M. Rinzan, S.G. Matsik, A.G.U. Perera, H.C. Liu, B.N. Zhonkov, V.I. Gavrilenko, A.A. Belyanin, J. Appl. Phys. 95 (2004) 512.
[12] D.G. Esaev, M.B.M. Rinzan, S.G. Matsik, A.G.U. Perera, J. Appl. Phys. 96 (2004) 4588.
[13] S.G. Matsik, M.B.M. Rinzan, A.G.U. Perera, H.C. Liu, Z.R. Wasilewski, M. Buchanan, Appl. Phys. Lett. 82 (2003) 139.
[14] A.G.U. Perera, S.G. Matsik, M.B.M. Rinzan, A. Weerasekara, M. Alevli, H.C. Liu, M. Buchanan, B. Zvonkov, V. Gavrilenko, Infrared Phys. Technol. 44 (2003) 347.
[15] W.J. Moore, J.A. Freitas Jr., R.J. Molnar, Phys. Rev. B 56 (1997) 12073.
[16] D.G. Esaev, S.G. Matsik, M.B.M. Rinzan, A.G.U. Perera, H.C. Liu, M. Buchanan, J. Appl. Phys. 93 (2003) 1879.
[17] H.F. Ghaemi, T. Thio, D.E. Grupp, T.W. Ebbesen, H.J. Lezec, Physical Review B 58 (1998) 6779–6782.
[18] M.I. Stockman, V.M. Shalaev, M. Moskovits, R. Botet, T.F. George, Physical Review B 46 (1992) 2821–2830.
[19] M.I. Stockman, Physical Review Letters 79 (1997) 4562–4565.
[20] M.I. Stockman, Physical Review Letters 84 (2000) 1011–1014.
[21] M. Ohtsu, K. Kobayashi, T. Kawazoe, S. Sangu, T. Yatsui, IEEE Journal of Selected Topics in Quantum Electronics 8 (2002) 839–862.
[22] R.W. Woods, Philo. Mag. 396 (1902) 396.
[23] V.V. Popov, T.V. Teperik, O.V. Polischuk, X.G. Peralta, S.J. Allen, N.J.M. Horing, M.C. Wanke, Phys. Solid State 46 (2004) 153.